TITLE: High-Throughput Global Phosphoproteomic Profiling Using Phospho Heavy-Labeled-Spiketide FAIMS Stepped-CV DDA (pHASED)

AUTHORS: Dilana E. Staudt[1,2], Heather C. Murray[1,2], David A. Skerrett-Byrne[3,4], Nathan D. Smith[5], Muhammad F. Jamaluddin[1], Richard G.S. Kahl[1], Ryan J. Duchatel[1,2], Zacary Germon[1,2], Tabitha McLachlan[1,2], Evangeline R. Jackson[1,2], Izac J. Findlay[1,2], Padraic S. Kearney[1,2], Abdul Mannan[1,2], Holly P. McEwen[1,2], Alicia M. Douglas[1], Brett Nixon[3,4], Nicole M. Verrills[1,2], Matthew D. Dun[1,2,*]

AFFILIATIONS:

[1]School of Biomedical Sciences and Pharmacy, College of Health, Medicine and Wellbeing, University of Newcastle, NSW, 2308, Australia

[2] Precision Medicine Program, Hunter Medical Research Institute, New Lambton Heights, NSW, 2305, Australia

[3] School of Environmental and Life Sciences, College of Engineering, Science and Environment, University of Newcastle, NSW, 2308, Australia

[4] Infertility and Reproduction Research Program, Hunter Medical Research Institute, New Lambton Heights, NSW, 2305, Australia

[5] ABRF, Research Services, University of Newcastle, NSW, 2308, Australia.

*** CORRESPONDING AUTHOR INFORMATION:** Matthew Dun, School of Biomedical Sciences and Pharmacy, College of Health, Medicine and Wellbeing, University of Newcastle, NSW, 2308, Australia. Ph: +61 4921 5693 Email: matt.dun@newcastle.edu.au

ABBREVIATIONS

ACN	acetonitrile
AKT1	RAC-alpha serine/threonine-protein kinase
AML	acute myeloid leukemia
ATM	Serine/threonine protein kinase ataxia-telangiectasia mutated
ATR	Serine/threonine-protein kinase ataxia- and Rad3-related
AURKB	Aurora kinase B
BCA	bicinchoninic acid
CSNK1D	Casein kinase I isoform delta
CSNK2A2	Casein kinase II subunit alpha
CV	compensation voltage
DDA	data dependent acquisition
DSB	double-strand breaks
DTT	dithiothreitol
FAIMS	high-field asymmetric waveform ion mobility spectrometry
FDR	false discovery rate
HCD	high-energy collision dissociation
HCl	hydrochloric acid
HILIC	hydrophilic interaction liquid chromatography
IPA	ingenuity pathway analysis
ITD	internal tandem duplications
KSEA	kinase-substrate enrichment analysis
LC	liquid chromatography
LFQ	label-free quantitation
m/z	mass-to-charge ratios
MS	mass spectrometry
nLC-MS/MS	nanoliquid chromatography–tandem mass spectrometry
NM	non-modified
NOX	NADPH oxidase

51	pHASED	Phospho Heavy-labeled-spiketide FAIMS Stepped-CV DDA
52	PI3K	phosphoinositide 3-kinase
53	PIKK	Phosphatidylinositol 3-kinase-related kinases (PIKKs)
54	PRKDC; DNA-PK	DNA-dependent protein kinase
55	PSM	phosphopeptide-spectrum matches
56	PTMs	posttranslational modifications
57	ROS	reactive oxygen species
58	RT	room temperature
59	SMG1	Nonsense mediated mRNA decay associated PI3K related kinase
60	SPE	solid phase extraction
61	TCA	trichloroacetic acid
62	TEAB	triethylammonium bicarbonate
63	TFA	trifluoroacetic acid
64	TiO2	titanium dioxide
65	TKI	tyrosine kinase inhibitors
66	TMT	tandem mass tag
67	UHMK1	Serine/threonine-protein kinase Kist

ABSTRACT

Global high-throughput profiling of oncogenic signaling pathways by phosphoproteomics is increasingly being applied to cancer specimens. Such quantitative unbiased phosphoproteomic profiling of cancer cells identifies oncogenic signaling cascades that drive disease initiation and progression; pathways that are often invisible to genomics sequencing strategies. Therefore, phosphoproteomic profiling has immense potential for informing individualized anti-cancer treatments. However, complicated and extensive sample preparation protocols, coupled with intricate chromatographic separation techniques that are necessary to achieve adequate phosphoproteomic depth, limits the clinical utility of these techniques. Traditionally, phosphoproteomics is performed using isobaric tagged based quantitation coupled with TiO_2 enrichment and offline prefractionation prior to nLC-MS/MS. However, the use of isobaric tags and offline HPLC limits the applicability of phosphoproteomics for the analysis of individual patient samples in real-time. To address these limitations, here we have optimized a new protocol, phospho-Heavy-labeled-spiketide FAIMS Stepped-CV DDA (pHASED). pHASED maintained phosphoproteomic coverage yet decreased sample preparation time and complexity by eliminating the variability associated with offline prefractionation. pHASED employed online phosphoproteome deconvolution using high-field asymmetric waveform ion mobility spectrometry (FAIMS) and internal phosphopeptide standards to provide accurate label-free quantitation data. Compared with our traditional tandem mass tag (TMT) phosphoproteomics workflow and optimized using isogenic FLT3-mutant acute myeloid leukemia (AML) cell line models (n=18/workflow), pHASED halved total sample preparation, and running time (TMT=10 days, pHASED=5 days) and doubled the depth of phosphoproteomic coverage in real-time (phosphopeptides = 7,694 pHASED, 3,861 TMT). pHASED coupled with bioinformatic analysis

predicted differential activation of the DNA damage and repair ATM signaling pathway in sorafenib-resistant AML cell line models, uncovering a potential therapeutic opportunity that was validated using cytotoxicity assays. Herein, we optimized a rapid, reproducible, and flexible protocol for the characterization of complex cancer phosphoproteomes in real-time, highlighting the potential for phosphoproteomics to aid in the improvement of clinical treatment strategies.

Word Count: 298

KEYWORDS: Phosphoproteomics, drug targets, oncogenic signaling, acute myeloid leukemia, cancer, pHASED, ATM, kinase signaling, clinical phosphoproteomics, resistance, therapy, combination therapy

INTRODUCTION

Mass spectrometry approaches for global high-throughput quantitation of cellular phosphoproteomes have been increasingly applied to cancer specimens as they provide powerful tools for the identification of signaling pathways including kinases, phosphatases and cell cycle regulators that drive disease initiation and progression (1-3). Deregulation of kinase and phosphatase activity plays a critical role in cancer development and relapse (4-7), highlighting kinases as important therapeutic targets in the clinic (8, 9). This is particularly the case for FLT3 kinase-driven acute myeloid leukemia (AML) patients. The FLT3 receptor tyrosine kinase is recurrently mutated in AML patients and is a target for FLT3 inhibitor therapy. The most common mutations are internal tandem duplications (ITD) and kinase domain mutations (e.g. D835). Resistance to FLT3 inhibitor therapy is often associated with the emergence of dual FLT3-ITD/D835 mutations, however the pathways mediating drug resistance are yet to be fully characterized (3, 5, 6). Therefore, phosphoproteomic profiling of the activated kinases responsible for driving downstream oncogenic signaling cascades using cancer patients' specimens in real-time, provides an opportunity to repurpose clinically relevant therapeutic interventions (10-14), and thus aid in the development of individualized treatment strategies that may improve overall survival.

Several methods have been developed for the quantitative characterization of phosphoproteins in complex biological samples using shotgun proteomics (15-18). Stable isotope-labeling strategies such as tandem mass tag (TMT) approaches have become increasingly popular due to the capability to multiplex analysis of up to 18 complex matrices simultaneously. TMT protocols enable samples to be pooled prior to nano liquid chromatography–tandem mass spectrometry (nLC-MS/MS) therefore saving instrument time and reducing technical variations in the

workflow. However, the highly complex nature of cancer phosphoproteomes necessitates that TMT protocols are coupled with phosphopeptide enrichment and sample pre-fractionation prior to nLC-MS/MS analysis in order to achieve adequate phosphoproteome resolution. Additionally, the high cost of reagents, fixed number of samples, and sample preparation time and complexity combine to limit the utility of TMT protocols for the ad hoc assessment of patient specimens in real-time.

Label-free quantitation (LFQ) strategies provide quantitative phosphoproteomic data without the use of isotopic-tags, mainly through the direct inference of protein abundance using the measured intensity of detected peptides, or indirect inference based on the number of phosphopeptide-spectrum matches (PSMs) obtained for each protein (19). LFQ protocols have the capacity to overcome some of the TMT-workflow limitations by reducing the complexity of sample preparation, saving both time and on costly reagents. Additionally, there is no limit to the number of matrices to be analyzed, thus enabling the comparison of larger sets of samples than when using label-based approaches. Such strategies therefore hold obvious appeal in the context of highly aggressive forms of cancer in which the design of appropriate treatment strategies is time-sensitive, and hence the ability to rapidly perform phosphoproteomic profiling on a high number of samples is of critical importance. However, label-free strategies have their own limitations, which include the inherent variability of individual sample preparation and loading, and the requisite number of replicates. Additionally, chromatographic conditions and the semirandom nature of data acquisition also have an impact on sample reproducibility (20). The addition (spike-in) of known concentrations of standard heavy-labeled exogenous phosphopeptides for sample normalization however, can help to overcome some of these limitations (16, 21), and therefore provides a strategy to normalize protein expression and

phosphorylation abundance from different cancer specimens analyzed at any time. Additionally, by interfacing phosphopeptide enrichment with separation via FAIMS prior to high-resolution mass spectrometry (MS) the collection of single-shot proteomic data is possible without the need to perform conventional two-dimensional liquid chromatography (2D-LC) approaches (22), and provides deep phosphoproteomic coverage to identify cancer-associated drug targets, in real-time.

In seeking to combine the salient features of these analytical modalities, here we report the optimization of a new protocol that employs online phosphoproteome deconvolution in tandem with LFQ in the presence of internal control heavy-labeled standards. This protocol was developed to identify kinases driving disease progression and therapy resistance in real-time. To determine the pre-clinical utility of this approach, pHASED was applied to isogenic FLT3-mutant AML cell lines resistant to the tyrosine kinase inhibitor sorafenib.

EXPERIMENTAL PROCEDURES

Cell Culture

Murine hematopoietic progenitor FDC-P1 cells were stably transduced with either human wildtype (WT) *FLT3*, *FLT3*-ITD, *FLT3*-D835Y, *FLT3*-D835V, *FLT3*-ITD/D835V, or *FLT3*-ITD/D835Y by retroviral transduction (6), confirmed by standard Sanger sequencing (Suppl Materials and Methods). FDC-P1 FLT3-transduced lines were maintained in standard culture conditions (5% CO_2, 37^{o}C) in DMEM medium (Thermo Fisher Scientific) with the addition of 10% FBS, and 20mM HEPES (N-2-hydroxyethylpiperazine-N'-2-ethanesulfonic acid). A total of 50 ng/mL human FLT3-ligand (Biolegend) was added to FLT3-WT cells, whereas FLT3-mutant lines are factor-independent and were therefore maintained in growth factor free media. All cell

lines were routinely confirmed to be free of mycoplasma contamination using a MycoAlert mycoplasma detection kit (Lonza; Basel, Switzerland).

Sample Preparation and Protein Extraction

TMT-based phosphopeptide quantification – Snap frozen transduced FDC-P1 cells expressing human wildtype-*FLT3* and AML associated FLT3-mutations were lysed in 100 µL of ice-cold 0.1 M Na_2CO_3, pH 11.3 containing protease and phosphatase inhibitors (Sigma, cat. #P8340-5ML, and #4906837001 respectively), by sonication (2 × 20 s cycles, 100% output power) (as described (23-25)). Protein concentration was determined using a Bicinchoninic acid (BCA) protein estimation assay, as per manufacturer's instructions (Thermo Fisher Scientific). Protein samples were then diluted in 6 M Urea/2 M Thiourea and reduced using 10 mM dithiothreitol (DTT) by incubation for 30 min at room temperature (RT). Reduced cysteine residues were then alkylated using 20 mM iodoacetamide by incubation for 30 min at RT in the dark. Enzymatic digestion was achieved using Trypsin/Lys-C mixture (Promega) at an enzyme-to-substrate ratio of 1:50 (w/w) and incubated for 3 h at RT. Triethylammonium bicarbonate (TEAB, 50 mM, pH 7.8) was then added to dilute urea concentration below 1 M, and samples were incubated overnight at RT. Lipid precipitation was performed using formic acid and trichloroacetic acid (TCA). Briefly, a final concentration of 2% formic acid was added to each sample, prior to centrifugation at 14,000 g for 10 min. Remaining lipopeptides were then precipitated with 20% (w/w) TCA and incubated on ice for at least 1 h prior to centrifugation. Pellets were washed with ice cold 0.01 M hydrochloric acid (HCl)/90% acetone and supernatants containing peptides were combined. Peptides were desalted using Oasis HLB solid phase extraction (SPE) cartridges and a VisiprepTM SPE Vacuum Manifold (12-port model; Sigma). The SPE cartridges were activated using 100% acetonitrile (ACN) and equilibrated using 0.1% trifluoroacetic acid (TFA). Acidified

192 samples (pH < 3) were loaded onto SPE cartridges with liquid passed through the solid phase
193 dropwise using vacuum pressure. The cartridges were washed with 0.1% TFA followed by
194 sequential elution of peptides using 60% ACN/0.1% TFA and 80% ACN/0.1% TFA. Eluted
195 peptides were then resuspended in TEAB (50 mM, pH 8) and quantitated using a peptide
196 fluorescence assay kit (Thermo Fisher Scientific). 100 µg from each of the samples were
197 individually labeled using tandem mass tags (Supplemental Table S1; TMT-10plex 3 × kits,
198 Thermo Fisher Scientific, Bremen DE, Germany) and mixed at a 1:1 ratio. Phosphopeptides were
199 isolated from the proteome using titanium dioxide (TiO_2) as previously described (11) before
200 offline hydrophilic interaction liquid chromatography (HILIC) using a Dionex Ultimate
201 3000RSLC nanoflow HPLC System (Thermo Fisher Scientific).

202 **pHASED** – peptide preparation was performed the same as for TMT and peptides desalted as
203 above. Following activation and equilibration, SPE cartridges were blocked with 33 µg of
204 trypsin-digested bovine serum albumin (BSA) peptides prior to sample clean-up. Peptides were
205 sequentially eluted using 60% ACN/0.1% TFA, and 80% ACN/0.1% TFA, and the eluates were
206 quantified using a Qubit 2.0 Fluorometer, as per manufacturer's instructions (Thermo Fisher
207 Scientific). A total of 200 µg of peptide per sample was utilized for TiO_2 enrichment. Spike-in
208 heavy-labeled phosphorylated peptides (Supplemental Table S2; including individually tyrosine,
209 threonine or serine phosphorylated heavy-labeled spiketides, 8 fmol/200 µg of sample) were
210 added as internal controls. Phosphopeptide enrichment was modified based on previous protocols
211 (11, 13, 18). In brief, each peptide sample was suspended in 80% ACN, 5% TFA, and 1 M
212 glycolic acid (loading buffer). TiO_2 beads were added at 0.6 mg per 100 µg peptide (w/w), and
213 samples were mixed at RT for 15 min. The supernatant was incubated with half the amount of
214 fresh TiO_2 beads, and resultant supernatants containing non-phosphorylated peptides (non-

modified = NM fraction) were removed and stored. The two sets of beads with bound phosphopeptides were pooled using 100 µL of loading buffer, followed by sequential washing with 80% ACN/1% TFA, and 10% ACN/0.1% TFA. Phosphopeptides were eluted with 28% ammonia hydroxide solution (1% v/v, pH 11.3) then passed through a C8 stage tip to remove residual beads (18). Phosphopeptides were lyophilized completely prior to resuspension in 2% ACN/0.1% TFA for nLC-MS/MS analysis.

Nanoflow Liquid Chromatography Tandem Mass Spectrometry Mass Spectrometry (nLC-MS/MS)

TMT-based phosphopeptide quantification – LC tandem mass spectrometry (MS/MS) was performed on 9 phosphopeptide enriched HILIC fractions using a Q-Exactive Plus hybrid quadrupole-Orbitrap MS system (Thermo Fisher Scientific) coupled to a Dionex Ultimate 3000RSLC nanoflow HPLC system (Thermo Fisher Scientific). Approximately 700 ng of phosphopeptide per HILIC fraction were loaded onto an Acclaim PepMap100 C18 75 µm × 20 mm trap column (Thermo Fisher Scientific) for pre-concentration and online desalting. Separation was then achieved using an EASY-Spray PepMap C18 75 µm × 25 cm column (Thermo Fisher Scientific) employing a linear gradient from 5 to 35% acetonitrile at 300 nL/min over 127 min. The Q-Exactive Plus MS System (Thermo Fisher Scientific) was operated in full MS/data- dependent acquisition MS/MS mode (DDA). The Orbitrap mass analyzer was used at a resolution of 70,000, to acquire full MS with an m/z range of 380–2000, incorporating a target automatic gain control value of $1e^6$ and maximum fill times of 50 ms. The 20 most intense multiply charged precursors were selected for higher-energy collision dissociation (HCD) fragmentation with a normalized collisional energy of 32. MS/MS fragments were measured at

an Orbitrap resolution of 35,000 using an automatic gain control target of $5e^5$ and maximum fill times of 120 ms.

pHASED – reverse phase nanoflow LC-MS/MS was performed using a Dionex Ultimate 3000RSLC nanoflow high-performance liquid chromatography system coupled with an Orbitrap Exploris 480 MS equipped with a front-end FAIMS Interface (Thermo Fisher Scientific). Approximately 700 ng of phosphopeptide per CV were loaded onto an Acclaim PepMap 100 C18 75 µm × 20 mm trap column for pre-concentration and online de-salting. Separation was then achieved using an EASY-Spray PepMap C18 75 µm × 25 cm, employing a gradient of 0-35% solvent B (solvent A = 0.1% formic acid, solvent B = 90% ACN, 0.1% formic acid) at a flow rate of 250 nL/min over 75 min. The mass spectrometer was operated in positive mode with the FAIMS Pro interface. Four compensation voltages (CV; -70, -60, -50, -40) were individually run for each biological triplicate. Full MS/data dependent acquisition (DDA) was performed using the following parameters: Orbitrap mass analyzer set at a resolution of 60,000, to acquire full MS with an m/z range of 350-1200, incorporating a standard automatic gain control target of $1e^6$ and maximum injection time of 50 ms. The 20 most intense multiply charged precursors were selected for higher-energy HCD with a collisional energy of 30. MS/MS fragments were measured at an Orbitrap resolution of 15,000 incorporating a normalized automatic gain control target of 250% and a maximum injection time of 120 ms.

Data Processing and Bioinformatic Analysis

Data analysis was performed using Proteome Discoverer (Thermo Fisher Scientific). Sequest HT was used to search against UniProt *Mus musculus* database (25,280 sequences, downloaded 30/05/20 for TMT; 17,462 sequences, downloaded 23/03/21 for pHASED) and *Homo sapiens* FLT3 FASTA file containing WT and mutant FLT3 sequences (3 sequences, downloaded

21/02/20 in both experiments). Database searching parameters included up to two missed cleavages, precursor mass tolerance set to 10 ppm and fragment mass tolerance of 0.02 Da. Cysteine carbamidomethylation was set as a fixed modification while dynamic modifications included oxidation (M), phosphorylation (S, T, Y), acetylation (K), methylation (K) and deamidation (N, Q). In addition, N-terminus TMT6plex was set as fixed modifications for TMT-labeled samples. Interrogation of the database was performed to evaluate the false discovery rate (FDR) of peptide identification based on q-values estimated from the target-decoy search approach using Percolator. An FDR rate of 1% was set at the peptide level to filter out target peptide spectrum matches over the decoy-peptide spectrum matches. Additionally for pHASED samples, heavy-labeled 13C(6)15N(2) (K), and 13C(6)15N(4) (R) modifications were included as dynamic modifications to identify spiked-in heavy-labeled phospho-spiketides. To account for variations in sample injection, reporter ion abundances were normalized to total peptide amount for the TMT-labeled protocol, and the spiked-in heavy-labeled phosphopeptides included as FASTA file for pHASED (Suppl Fig. S1). For quantification and comparison, each ratio was transformed to log2 scale (log2 ratio).

Experimental Design and Statistical Rationale

Phosphoproteomic data analysis was performed using six FDC-P1 isogenic cell lines (n=3 biological replicates). Four compensation voltages (CV; -70, -60, -50, -40) were individually analyzed for each biological replicate. Differentially expressed phosphopeptides and phosphorylation sites were defined as those with a significant ($p \leq 0.05$) log2 fold change ≥ 0.25 or ≤ -0.25. Differences between sample groups were analyzed by unpaired Student's t-tests or one-way ANOVA and considered significant when $p \leq 0.05$. Graphical data was analyzed and

prepared using Perseus (1.6.2.2), String (11.5), CytoScape (3.9.1), and GraphPad Prism (9.0.1). Results are presented as mean values ± SEM.

Ingenuity Pathway Analysis

Ingenuity Pathway Analysis software (IPA; Qiagen) was used to analyze each phosphoproteomic dataset (as previously described (11, 13)). Canonical pathways, upstream regulators, and disease and function analyses were generated and assessed based on *p*-value.

Kinase-Substrate Enrichment Analysis

Kinase-Substrate Enrichment Analysis (KSEA App, version 1.0) (26) was used to analyze phosphorylated sites based on PhosphoSitePlus (27) kinase-substrate dataset, and a $p \leq 0.05$ cut-off.

Cytotoxicity Assays

Cell lines were treated with the FLT3 inhibitor sorafenib (Selleckchem) (28), and ATM inhibitor KU-60019 (Selleckchem) (29) either alone or in combination. Cells were seeded into 96 well plates at $2e^4$ cells per well, and viability following treatments was measured using Resazurin (excitation 544 nm, emission 590 nm; 0.6 mM Resazurin, 78 µM Methylene Blue, 1 mM potassium hexacyanoferrate (III), 1 mM potassium hexacyanoferrate (II) trihydrate (Sigma), dissolved in sterile phosphate buffered saline). Synergy of dose-response and combined effect of the two drugs were assessed using the method of Bliss independence model (30).

RESULTS

pHASED reduced sample preparation time by half whilst providing improved phosphopeptide quantification compared to the TMT workflow

The new label-free phosphoproteomic enrichment and MS protocol 'pHASED' described herein, couples phosphopeptide enrichment strategies optimized by Engholm-Keller et.al., (2012) (18) and LFQ using heavy-labeled internal phospho-spiketides and FAIMS interface optimized by Alexander et.al., (2018) (22), to decrease sample preparation time and increase phosphoproteome deconvolution and coverage for the analysis of samples in real-time (Fig. 1). We performed initial comparison of our optimized pHASED with traditional TMT phosphoproteomic protocols using six isogenic cell line models of FLT3-mutant AML in biological triplicate (Table 1; n = 36 samples). The sample preparation in pHASED saves time due to the substitution of TMT-labeling with the spike-in of heavy-labeled phospho-spiketides of known concentration in order to normalize sample injection and phosphopeptide quantitation. We replaced offline HILIC for online deconvolution using FAIMS interface employing external stepping of four different compensation voltages (CV; -70, -60, -50, -40) over a 75 min gradient. Individual sample injection per CV provided more flexibility to the experiment, however, increased LC-MS/MS time by 1.4 days (2 days TMT; 4 days pHASED). This longer instrument time however, is compensated by the reduction of sample preparation time by half, requiring an overall ~5 days for completion of pHASED experiment, whereas ~10 days are required for TMT (Fig. 1*A*, 1*B*).

To determine the utility of each protocol, we examined the PSMs of each experiment (Fig. 2). Analysis of the charge states (Fig. 2*A*) and precursor ion mass-to-charge ratios (m/z) (Fig. 2*B*) for the two protocols demonstrated that our traditional TMT approach identified a higher percentage of +2 and +3 charged precursor ions, ranging between 400-700 m/z, whereas pHASED identified a greater number of +4, +5, and +6 precursors and higher m/z ratios (700-1200). The fractionation profile of the four CVs applied in pHASED were analyzed by comparing the PSMs acquired in each CV (Fig. 2*C-F*). More unique PSMs were identified in

lower CVs, such as -70V and -60V compared to -50V and -40V (Fig. 2*C*). Interestingly, similar FAIMS distributions were seen for phosphopeptides as previously reported for studies employing FAIMS to characterize the non-modified proteome (22). For most charge states, the lower the CV the lower the average m/z (Fig. 2*D*, 2*E*), except for +6 charged precursors, which showed similar average m/z across CVs (Fig. 2*E*). Analysis of the overlapping distributions of common and unique phosphoproteins identified showed deep phosphoproteome coverage across all four CVs (Fig. 2*F*) (31).

To examine the reproducibility of the quantification achieved using TMT and pHASED we performed Pearson Correlation analysis of the biological replicates (n=3) across each cell line (n=6) (Fig. 3). Correlation was performed by plotting normalized phosphopeptide abundances from each biological replicate per sample in a correlation matrix. This analysis revealed increased quantification reproducibility in all biological replicates of samples analyzed with pHASED (Fig. 3*A*, 3*C*) in comparison to the TMT protocol (Fig. 3*B*, 3*C*), which presented a moderate correlation between replicates and samples. These results indicate that, in our hands, pHASED performed as a more consistent phosphopeptide quantification tool, and therefore may yield more biologically relevant data.

pHASED provided in-depth phosphoproteome coverage

Our TMT approach identified 1,958 phosphoproteins and 3,861 phosphorylated peptides (FDR 1%), whereas a total of 1,587 phosphoproteins and 7,694 phosphorylated peptides were identified using pHASED (FDR 1%) (Fig. 4*A*, Supplemental Tables S*3*, S*4*). Both protocols identified similar S:T:Y ratios, in accordance with previous findings reporting a phosphorylation ratio of 86:12:2 (%) (32). The overall success of phosphopeptide enrichment for each experiment was 72% for TMT, and 93% for pHASED (Fig. 4*A*), indicating good enrichment efficiency in

both experiments. Furthermore, pHASED identified an overall higher number of multi-phosphorylated peptides (2,800 singly-, 1,348 doubly-, and 323 triply- phosphorylated peptides, FDR 1%) compared to our traditional TMT approach (2,069 singly-, 334 doubly-, and 11 triply-phosphorylated peptides, FDR 1%) (Fig. 4*B*). Notably, overall increased phosphoprotein coverage and identification of more peptides per protein was achieved by pHASED (Fig. 4*C*, 4*D*). Comparison between identified phosphoprotein accessions across all datasets showed a 47% overlap between pHASED and TMT (Fig. 4*E*, and Supplemental Table S*5)*.

Both pHASED and TMT identified similar numbers of hydrophobic peptides, with both protocols preferencing the identification of hydrophilic phosphopeptides (Fig. 4*F*). For quantification, normalization of TMT samples was achieved based on total peptide amount per TMT channel, whereas each sample analyzed by pHASED was normalized with spike-in phospho-spiketides of known concentration. Measured abundance ratios were then transformed to log2 scale (log2 ratio). The distribution of phosphopeptide log2 fold-changes comparing FLT3 mutant sample to FLT3-wt cell lines measured by pHASED showed a greater dynamic range than those measured by TMT-based quantification (Fig. 4*G*), with a mean of log2 fold-change closer to 0 for all cell lines in the TMT approach compared to pHASED (mean log2 1.29; p=0.0002).

pHASED identified relevant therapeutic drug targets in drug resistant AML

pHASED and TMT identified similar numbers of phosphoproteins with kinase activity (Fig. 4*H; 1% FDR*). In accordance with our previous findings of divergencies between the number of identified phosphoproteins in TMT compared to pHASED (Fig. 4*E*), 39% of kinases were identified to be common to both analyses (Supplemental Tables S*6-8*). Despite differences, the numbers of kinases identified showed that both protocols were effective for the identification of

clinically relevant drug targets that could potentially aid in the design of treatment strategies for cancer patients. Analysis of the phosphorylation profile of kinases identified in FLT3-ITD, resistant FLT3-ITD/D835V, and resistant FLT3-ITD/D835Y cell lines was performed to investigate the clinical utility of pHASED, and results were compared to our TMT approach (Fig. 5). FLT3-ITD mutations are seen in approximately 27% of AML patients at diagnosis and are associated with a high risk of relapse (3). Resistance to commonly used FLT3 inhibitors including sorafenib (33-39) (Supplemental Table S*9*) occurs following FLT3-ITD+ AML cells acquiring a secondary point mutation in the kinase domain of FLT3 (FLT3-ITD/D835V and FLT3-ITD/D835Y, henceforth referred to as "double mutant"). Cytotoxicity assays using the FLT3 inhibitor sorafenib confirmed the resistant phenotype of FLT3-ITD/D835V and FLT3-ITD/D835Y mutants (Fig. 5*A*), which presented an average 47-fold increase in sorafenib IC_{50} in comparison to FLT3-ITD cell lines (IC_{50} 4.2 µM, 2.7 µM, 0.073 µM, FLT3-ITD/D835V, FLT3-ITD/D835Y and FLT3-ITD respectively). pHASED identified a significantly increased number of kinases that showed differential phosphorylation in both resistant cell lines in comparison to the TMT approach, particularly in FLT3-ITD/D835Y mutants (Fig 5*B; p*=0.0009). In addition, analysis of kinases showing significantly altered phosphorylation in double mutants compared with FLT3-ITD cells (log2 +/- 0.25; $p \leq 0.05$) showed greater dynamic range via pHASED compared to TMT (Fig. 5*C*).

Protein-protein interaction network analysis of kinases identified in TMT and pHASED (log2 +/-0.25) revealed the enrichment of clustered kinases associated with signaling pathways that are known to be commonly deregulated in cancer (Fig. 5*D*-*G*). Both datasets identified kinases associated with, Signal Transduction, RAF (40) and ERK/MAPK (41) signaling (Fig. 5*D*-*G*), in line with previous studies that show potent activation of this oncogenic signaling pathway drives

resistance to sorafenib (42). In addition, across resistance models, pHASED identified kinases responsible for controlling cell cycle and p53 signaling (43) (Fig. 5*D*, 5*E*), whereas TMT identified kinases associated with NFkB signaling (44) (Fig 5*F*, 5*G*).

pHASED identified divergent DNA damage and repair pathways associated with sorafenib resistance in FLT3-mutant AML

Kinase-substrate enrichment analysis (KSEA) of TMT and pHASED datasets comparing resistant to diagnosis cells, predicted activation of oncogene RAC-alpha serine/threonine-protein kinase (AKT1), cell cycle regulators Cyclin dependent kinase 16 (CDK16), Polo-like kinase 2/3 (PLK2, PLK3), Serine/threonine-protein kinase VRK1/2 (VRK1/2), and Serine/threonine-protein kinase Kist (UHMK1); and DNA damage sensor and repair associated DNA-dependent protein kinase (PRKDC, or DNA-PK) (Fig. 6*A*, Supplemental Tables S*10*, S*11*). Furthermore, IPA analysis of canonical pathways associated with resistance (Fig. 6*B*, Supplemental Tables S*12*, S*13*) uncovered cell cycle regulation (Cell cycle control of Chromosomal Replication, G1/S and G2/M checkpoints, and Cyclins and Cell Cycle Regulation), and DNA damage and repair (ATM, NER, p53 and BRCA1, p-value <0.001) signaling as among the most significant enriched canonical pathways in resistant cell lines. Both mutants were also enriched for FLT3, and AML associated signaling pathways such as ERK/MAPK, JAK/STAT, mTOR, and PI3K/AKT, although with less statistical power (increased p-value ≤0.05).

The Serine/threonine protein kinase (ATM) regulates response to DNA damage caused by double-strand breaks (DSBs) (13). ATM is member of the phosphoinositide 3-kinase (PI3K)-related protein kinase (PIKK) family, and signals through DNA damage response kinases ATR, DNA-PKcs and Nonsense Mediated MRNA Decay Associated PI3K Related Kinase (SMG1) (45, 46). One potent mechanism of increased DSBs is via the excess production of reactive

oxygen species (ROS). Increased ROS production by the NADPH oxidase (NOX) family of enzymes in acute leukemias, particularly FLT3-ITD AML, has been increasingly studied over the last few years, and highlights that elevated ROS is a mechanism conferring survival advantages in FLT3-mutant AML (47-50). Given ATM signaling was predicted to be one of the top ranked canonical pathways driving the DNA damage repair and response pathways in resistant cells (Fig. 6*B*), we chose to analyze this pathway to test the biological utility of the phosphoproteomic analysis generated via pHASED in FLT3-ITD/D835V and FLT3-ITD/D835Y mutant cells.

Analysis of ATM (Fig. 6*C*) and DSB repair phosphoproteins (Fig 6*D*, 6*E*) in resistant models using pHASED, revealed divergent phosphorylation profiles. In FLT3-ITD/D835V mutant cells, pHASED only identified significantly increased phosphorylation of DSB repair pathway phosphoprotein UBA1 (S4) (log2 0.59; p=0.037) (Fig. 6*D*). Whereas, in FLT3-ITD/D835Y mutant cells, pHASED identified significantly increased phosphorylation of phosphoproteins downstream of ATM kinase signaling including CDKN1A (S78) (log2 1.62; p=0.034), TOPBP1 (S862, S863) (log2 1.00; p=0.048) and TRIM28 (S594) (log2 2.06; p=0.04) (Fig. 6*C*). Additionally, increased phosphorylation of three phosphopeptides for SFR1 (S67, S83, S99; S67, S71, S83, S87, S99, S103; and S115) (log2 1.93, p=0.003; log2 1.88 p=0.010; and log2 2.02 p=0.028, respectively), DYRK1A (Y321) (log2 0.88; p=0.03), two phosphopeptides for NUCKS1 (S58, S61; and S181) (log2 4.07, p=0.0009; and log2 1.28, p=0.04, respectively), and PDS5B (S1356) (log2 1.84; p=0.022) were identified in FLT3-ITD/D835Y mutant cells, highlighting the unique mechanisms of DNA repair regulation in this resistance model (Fig. 6*E*). These data add further evidence to pathway analysis divergencies shown using KSEA (Fig. 6*A*) and IPA canonical pathways association analysis comparing the double mutants (Fig. 6*A*).

Combined inhibition of ATM and FLT3 showed synergistic effect in sorafenib-resistant cell lines

Combination cytotoxicity analysis using the ATM inhibitor KU-60019 (29) in combination with the FLT3 inhibitor sorafenib (28) was highly synergistic, particularly in cells harboring the sorafenib resistance mutation FLT3-ITD/D835Y (Fig. 7). In accordance with pathway prediction bioinformatic analyses (Fig. 6), FLT3-ITD/D835Y mutant cells showed increased sensitivity to the combination, resensitizing cells to sorafenib (Fig. 7*A*, Bliss synergy analysis score 12.42; 0.062 μM sorafenib, 1.25 μM KU-60019); whereas FLT3-ITD/D835V mutant cells showed maximal synergy at higher doses (Fig. 7*B*, Bliss score 10.71; 500 nM sorafenib, 2.5 μM KU-60019). The combined inhibition of ATM and FLT3 signaling was only additive in FLT3-ITD mutant cells (Bliss score 5.20) with these cells highly sensitive to sorafenib alone (Fig. 5*A*, 7*C*). To test the *in vitro* preclinical benefits using physiological concentrations of sorafenib, cell survival comparisons were performed at 0.062 μM sorafenib. Again, these data confirmed the increased synergistic effects of combined ATM and FLT3 inhibition in FLT3-ITD/D835Y mutant cells (Fig. 7*D*) compared with FLT3-ITD/D835V mutant cells (Fig. 7*E*). Together, these results confirm that ATM inhibition plays a role in the resensitization of FLT3-ITD/D835 mutant resistant cells to sorafenib, validating the pHASED phosphoproteomic prediction of the important role ATM signaling plays in signaling downstream of the FLT3-ITD/D835Y mutation.

DISCUSSION

Proteomics and phosphoproteomics have been acknowledged as being among the most effective strategies to predict drug sensitivities (1, 51). However, we are yet to establish phosphoproteomic profiling in the clinical setting, or even to provide such as an additive

463 resource to genomically predicted therapeutic strategies; the establishment of which would
464 represent a pivotal advance in precision-medicine treatment regimens. Clinical
465 phosphoproteomic profiling also has enormous potential to identify treatment targets that are
466 invisible to genomics approaches, or to be used as an indicator of prognosis in the *de novo* and
467 refractory settings, in real-time. Indeed, the optimization of pHASED reported herein, goes some
468 way to moving phosphoproteomics from the discovery laboratory to that of the well-equipped
469 pathologist. Importantly, the reduced complexity and sample preparation time of pHASED
470 provides users with the capacity to prepare and sequence the phosphoproteomics of any
471 biological system in less than a week. Furthermore, pHASED provided accurate LFQ and online
472 deconvolution using FAIMS, whilst maintaining deep phosphoproteomic coverage without the
473 need for offline 2D-LC techniques.

474 FAIMS was initially and elegantly optimized to provide single-shot LC-MS/MS results
475 that compared favorably with 2D-LC fractionation experiments (22). Specifically, FAIMS was
476 first reported in the context of analyzing the non-modified proteome of a cell line established
477 from a chronic myelogenous leukemia patient (K562). In this study, the use of six CVs during a
478 six-hour single-shot FAIMS experiment identified 8,007 non-modified proteins; comparable to
479 the 7,776 non-modified proteins identified by the use of four 2D-LC fractionated samples, each
480 analyzed for 1.5 h. Here, we have optimized 5 h of FAIMS using four CVs identifying 1,587
481 quantified phosphoproteins using pHASED, compared to nine 2D-LC fractions sequenced over
482 ~19 h, which identified and quantified 1,958 phosphoproteins using a TMT approach.

483 Although TMT identified more unique phosphoproteins than pHASED, it is well
484 established that the use of isobaric tags can compromise identification efficiency due to peptide
485 ratio compression artifacts caused by coeluting ions alongside that of the precursor ion of the

peptide of interest; a phenomenon that interferes with MS2 based reporter ion quantitation (19, 52). Hence, this can limit the dynamic range of quantitation, and can often underrepresent the biological variability that exists between samples, especially for low abundant proteins (11, 53). Furthermore, the use of isobaric tags alters charge states during electrospray ionization (54), with the cleavage and loss of isobaric tags during MS2 generating fragment ions that complicate spectral interpretation by database searching algorithms (55), contributing to reduced identification efficiency. This was again evidenced by comparing phosphopeptide changes in FLT3-mutant AML models (n=5) with that of isogenic cell lines transduced to express the wt-FLT3 receptor (n=1), where the log2 fold-change of the TMT experiment was 0, compared with pHASED which showed an average log2 fold-change of 1.29 (p=0.0002). The biological differences revealed by pHASED further highlight the observation that knock in of each of the FLT3-mutations induced autonomous growth of isogenic cell lines, whereas cell lines transduced to express the wt-FLT3 receptor, required supplementation of growth factors to maintain growth and survival (5, 6, 56).

It was also of interest to note that pHASED identified more unique phosphosites per phosphoprotein compared to TMT. The biological context of this result was investigated by analyzing signaling pathways identified by both MS approaches to determine whether the increased number of identified phosphosites provided molecular insights relevant to the dissection of therapeutic vulnerabilities. Indeed, using both TMT and pHASED, IPA predicted ATM signaling to show increased activity in both FLT3-ITD/D835V and FLT3-ITD/D835Y double mutant cell line models compared to cells harboring FLT3-ITD mutations alone. ATM plays a functional role in the cellular response to DNA DSBs. Here it protects the cell against genotoxic stress, but, in cancer cells, helps to drive resistance to anticancer therapies thus

509 favoring leukemic growth and survival (57). Therefore, it is unsurprising that ATM signaling
510 may play a role in resistance to sorafenib in cells harboring double mutant FLT3-ITD/D835.
511 However, sorafenib is not only a potent inhibitor of wt-FLT3 and FLT3-ITD, but also inhibits
512 other receptor tyrosine kinases including VEGFR, PDGFR, KIT and RET, as well as
513 downstream serine/threonine kinases including RAF/MEK/ERK (28). Indeed, in sorafenib-
514 resistant double mutant FLT3-ITD/D835 cells, significantly increased MEK/ERK signaling was
515 predicted when compared with the phosphoproteomes of FLT3-ITD mutant cells, thereby
516 helping to explain the 47-fold increase in IC_{50} seen between the cell types. In glioma cells, ATM
517 inhibitors increased radiotherapy sensitivity (29, 58, 59), with ATM signaling through the
518 RAF/MEK/ERK pathway critical for radiation-induced ATM activation, suggestive of a
519 regulatory feedback loop between ERK and ATM (60). Sorafenib dose-dependently induced the
520 generation of ROS in tumor cells *in vitro* and *in vivo* (61), and hence it is highly possible that in
521 FLT3-ITD/D835 double mutants, RAF/MEK/ERK signaling through ATM helps to maintain
522 proliferation and promote DNA repair, even under situations of genotoxic stress induced by high
523 dose sorafenib.

524 pHASED identified more significant phosphorylation changes in ATM substrates in
525 FLT3-ITD/D835Y cells compared to FLT3-ITD/D835V cells ($p \leq 0.05$). Combination
526 cytotoxicity assays revealed significantly increased synergy between sorafenib and the ATM
527 inhibitor KU-60019 at physiologically relevant doses (most strikingly in FLT3-ITD/D835Y
528 cells) providing a treatment paradigm for patients harboring sorafenib resistance. The increased
529 phosphosite coverage arising from pHASED analyses potentially provides a more accurate
530 indication of the regulation of the ATM signaling pathway, and hence highlights mechanisms

promoting resistance to sorafenib (12); information that can be exploited to tailor effective preclinical treatment strategies.

Although pHASED may afford the opportunity to perform an unrestricted number of analyses (of benefit in the clinical setting where cancer diagnosis may not follow a predictable schedule), there remains important questions on how phosphoproteomics would be practically implemented as a clinical decision-making tool. For example, consideration needs to be given to sample processing time and the methods of patient sample collection; the phosphoproteome of leukemic blasts isolated from the bone marrow will differ from that sequenced from leukemic blasts isolated from peripheral blood. Additionally, the steps taken to enrich leukemic blasts following bone marrow trephine biopsy or phlebotomy are to be considered as alterations in signaling pathway activity can be influenced simply by the culture media used, or even the type of blood tube used at the time of sample collection (25), necessitating optimization and standardization of workflows. Importantly, for phosphoproteomics to aid in the treatment of cancer, the assessment of which pathways should be targeted and by which drugs needs to be evaluated under clinical trial conditions, like those testing whole genome sequencing (WGS) and RNA sequencing (RNAseq) strategies, in order to ensure robust recommendations can be made given phospho/proteomic data generated via pHASED (62).

In summary, the data obtained in the present study provides a novel method for LFQ of high-throughput phosphoproteomic data that maintains deep phosphoproteomic coverage without the need for complex 2D-LC strategies. pHASED provides the flexibility to analyze samples as they present and is not limited by the number of analyses that can be performed. Reduced time and complexity in sample preparation, and the optimization of online phosphoproteome deconvolution using a stepped CV FAIMS interface, provided accurate and reproducible

phosphoproteomes of complex cancer cells in less than a week. Moreover, pHASED successfully identified novel drug targets and potential therapeutic strategies to treat AML models resistant to therapies used in the clinic; optimized technologies that we hope will help in the rapid characterization of highly aggressive forms of cancer, as an important step towards improving treatment outcomes for cancer sufferers.

Word Count 5526

ACKNOWLEDGMENTS

This study was supported by Cancer Institute NSW Fellowships (M.D.D., N.MV). M.D.D. is supported by an NHMRC Investigator Grant – GNT1173892. This project is supported by an NHMRC Ideas Grant APP1188400 and NHMRC Targeted Research Grant GA65801. The contents of the published material are solely the responsibility of the research institutions involved or individual authors and do not reflect the views of NHMRC. D.S. and T.M. are supported by Zebra Equities Ph.D. Scholarships. Grants from the Hunter Medical Research Institute, Hunter Children's Research Foundation, Jurox Animal Health, Zebra Equities, Hunter District Hunting Club and Ski for Kids, and The Estate of James Scott Lawrie supported this work. The Cancer Institute NSW in partnership with the Faculty of Health and Medicine from the University of Newcastle funded the MS platform. Figure 1 was created with BioRender.com

AUTHOR CONTRIBUTIONS:

Contribution: D.E.S., and M.D.D., conceived and designed the study and interpreted the results. D.E.S., H.C.M, D.A.S.B., N.D.S., M.F.J., R.S.K., R.J.D., Z.P.G., T.M., E.R.J., I.J.F., P.S.K., A.M., H.P.M., and M.D.D., conducted the experiments and performed data analysis. A.M.D., B.N., and N.M.V., provided discipline specific expertise; D.E.S., and M.D.D., wrote and edited the manuscript. All authors discussed the results and commented on the manuscript.

DATA AVAILABILITY

The mass spectrometry proteomics data have been deposited to the ProteomeXchange Consortium (http://proteomecentral.proteomexchange.org) via the PRIDE partner repository (63) with the dataset identifier PXD032204 (TMT); and PXD032296 (pHASED).

PRIDE Reviewer account details:

TMT:

Username: reviewer_pxd032204@ebi.ac.uk

Password: tGkAKsrp

pHASED:

Username: reviewer_pxd032296@ebi.ac.uk

Password: 9yGk4Lrt

REFERENCES

1. Findlay, I. J., De Iuliis, G. N., Duchatel, R. J., Jackson, E. R., Vitanza, N. A., Cain, J. E., Waszak, S. M., and Dun, M. D. (2022) Pharmaco-proteogenomic profiling of pediatric diffuse midline glioma to inform future treatment strategies. *Oncogene* 41, 461-475
2. Duchatel, R. J., Jackson, E. R., Alvaro, F., Nixon, B., Hondermarck, H., and Dun, M. D. (2019) Signal Transduction in Diffuse Intrinsic Pontine Glioma. *Proteomics* 19, e1800479
3. Staudt, D., Murray, H. C., McLachlan, T., Alvaro, F., Enjeti, A. K., Verrills, N. M., and Dun, M. D. (2018) Targeting Oncogenic Signaling in Mutant FLT3 Acute Myeloid Leukemia: The Path to Least Resistance. *Int J Mol Sci* 19
4. Cicenas, J., Zalyte, E., Bairoch, A., and Gaudet, P. (2018) Kinases and Cancer. *Cancers (Basel)* 10
5. Dun, M. D., Mannan, A., Rigby, C. J., Butler, S., Toop, H. D., Beck, D., Connerty, P., Sillar, J., Kahl, R. G. S., Duchatel, R. J., Germon, Z., Faulkner, S., Chi, M., Skerrett-Byrne, D., Murray, H. C., Flanagan, H., Almazi, J. G., Hondermarck, H., Nixon, B., De Iuliis, G., Chamberlain, J., Alvaro, F., de Bock, C. E., Morris, J. C., Enjeti, A. K., and Verrills, N. M. (2020) Shwachman-Bodian-Diamond syndrome (SBDS) protein is a direct inhibitor of protein phosphatase 2A (PP2A) activity and overexpressed in acute myeloid leukaemia. *Leukemia* 34, 3393-3397
6. Smith, A. M., Dun, M. D., Lee, E. M., Harrison, C., Kahl, R., Flanagan, H., Panicker, N., Mashkani, B., Don, A. S., Morris, J., Toop, H., Lock, R. B., Powell, J. A., Thomas, D., Guthridge, M. A., Moore, A., Ashman, L. K., Skelding, K. A., Enjeti, A., and Verrills, N. M. (2016) Activation of protein phosphatase 2A in FLT3+ acute myeloid leukemia cells enhances the cytotoxicity of FLT3 tyrosine kinase inhibitors. *Oncotarget* 7, 47465-47478
7. Toop, H. D., Dun, M. D., Ross, B. K., Flanagan, H. M., Verrills, N. M., and Morris, J. C. (2016) Development of novel PP2A activators for use in the treatment of acute myeloid leukaemia. *Org Biomol Chem* 14, 4605-4616
8. Cohen, P., Cross, D., and Jänne, P. A. (2021) Kinase drug discovery 20 years after imatinib: progress and future directions. *Nature Reviews Drug Discovery* 20, 551-569
9. Bhullar, K. S., Lagarón, N. O., McGowan, E. M., Parmar, I., Jha, A., Hubbard, B. P., and Rupasinghe, H. P. V. (2018) Kinase-targeted cancer therapies: progress, challenges and future directions. *Molecular Cancer* 17, 48
10. Dun, M. D., Chalkley, R. J., Faulkner, S., Keene, S., Avery-Kiejda, K. A., Scott, R. J., Falkenby, L. G., Cairns, M. J., Larsen, M. R., Bradshaw, R. A., and Hondermarck, H. (2015) Proteotranscriptomic Profiling of 231-BR Breast Cancer Cells: Identification of Potential Biomarkers and Therapeutic Targets for Brain Metastasis * [S]. *Molecular & Cellular Proteomics* 14, 2316-2330
11. Degryse, S., de Bock, C. E., Demeyer, S., Govaerts, I., Bornschein, S., Verbeke, D., Jacobs, K., Binos, S., Skerrett-Byrne, D. A., Murray, H. C., Verrills, N. M., Van Vlierberghe, P., Cools, J., and Dun, M. D. (2018) Mutant JAK3 phosphoproteomic profiling predicts synergism between JAK3 inhibitors and MEK/BCL2 inhibitors for the treatment of T-cell acute lymphoblastic leukemia. *Leukemia* 32, 788-800
12. Murray, H. C., Dun, M. D., and Verrills, N. M. (2017) Harnessing the power of proteomics for identification of oncogenic, druggable signalling pathways in cancer. *Expert Opinion on Drug Discovery* 12, 431-447
13. Murray, H. C., Enjeti, A. K., Kahl, R. G. S., Flanagan, H. M., Sillar, J., Skerrett-Byrne, D. A., Al Mazi, J. G., Au, G. G., de Bock, C. E., Evans, K., Smith, N. D., Anderson, A., Nixon, B., Lock, R. B., Larsen, M. R., Verrills, N. M., and Dun, M. D. (2021) Quantitative phosphoproteomics uncovers synergy between DNA-PK and FLT3 inhibitors in acute myeloid leukaemia. *Leukemia* 35, 1782-1787
14. Duchatel, R. J., Mannan, A., Jackson, E. R., Staudt, D., Skerrett-Byrne, D. A., Jamaluddin, M. F. B., Woldu, A. S., Douglas, A., Hulleman, E., Carcaboso, A. M., Monje, M., Alvaro, F., Tsoli, M., Ziegler, D. S., and Dun, M. D. (2020) DIPG-29. PHOSPHATIDYLINOSITOL-4,5-BISPHOSPHATE 3-KINASE (PI3K) INHIBITION DRIVES PROTEIN KINASE C ACTIVATION (PKC) IN DIFFUSE INTRINSIC PONTINE GLIOMA (DIPG). *Neuro-Oncology* 22, iii292-iii293
15. Domon, B., and Aebersold, R. (2006) Mass spectrometry and protein analysis. *Science* 312, 212-217
16. Ong, S. E., and Mann, M. (2005) Mass spectrometry-based proteomics turns quantitative. *Nat Chem Biol* 1, 252-262
17. Ong, S. E., Blagoev, B., Kratchmarova, I., Kristensen, D. B., Steen, H., Pandey, A., and Mann, M. (2002) Stable isotope labeling by amino acids in cell culture, SILAC, as a simple and accurate approach to expression proteomics. *Mol Cell Proteomics* 1, 376-386

18. Engholm-Keller, K., Birck, P., Størling, J., Pociot, F., Mandrup-Poulsen, T., and Larsen, M. R. (2012) TiSH--a robust and sensitive global phosphoproteomics strategy employing a combination of TiO2, SIMAC, and HILIC. *J Proteomics* 75, 5749-5761
19. Bantscheff, M., Lemeer, S., Savitski, M. M., and Kuster, B. (2012) Quantitative mass spectrometry in proteomics: critical review update from 2007 to the present. *Analytical and Bioanalytical Chemistry* 404, 939-965
20. Li, Z., Adams, R. M., Chourey, K., Hurst, G. B., Hettich, R. L., and Pan, C. (2012) Systematic Comparison of Label-Free, Metabolic Labeling, and Isobaric Chemical Labeling for Quantitative Proteomics on LTQ Orbitrap Velos. *Journal of Proteome Research* 11, 1582-1590
21. Čuklina, J., Lee, C. H., Williams, E. G., Sajic, T., Collins, B. C., Rodríguez Martínez, M., Sharma, V. S., Wendt, F., Goetze, S., Keele, G. R., Wollscheid, B., Aebersold, R., and Pedrioli, P. G. A. (2021) Diagnostics and correction of batch effects in large-scale proteomic studies: a tutorial. *Molecular Systems Biology* 17, e10240
22. Hebert, A. S., Prasad, S., Belford, M. W., Bailey, D. J., McAlister, G. C., Abbatiello, S. E., Huguet, R., Wouters, E. R., Dunyach, J.-J., Brademan, D. R., Westphall, M. S., and Coon, J. J. (2018) Comprehensive Single-Shot Proteomics with FAIMS on a Hybrid Orbitrap Mass Spectrometer. *Analytical Chemistry* 90, 9529-9537
23. Dun, M. D., Chalkley, R. J., Faulkner, S., Keene, S., Avery-Kiejda, K. A., Scott, R. J., Falkenby, L. G., Cairns, M. J., Larsen, M. R., Bradshaw, R. A., and Hondermarck, H. (2015) Proteotranscriptomic Profiling of 231-BR Breast Cancer Cells: Identification of Potential Biomarkers and Therapeutic Targets for Brain Metastasis. *Mol Cell Proteomics* 14, 2316-2330
24. Nixon, B., Johnston, S. D., Skerrett-Byrne, D. A., Anderson, A. L., Stanger, S. J., Bromfield, E. G., Martin, J. H., Hansbro, P. M., and Dun, M. D. (2019) Modification of Crocodile Spermatozoa Refutes the Tenet That Post-testicular Sperm Maturation Is Restricted To Mammals. *Mol Cell Proteomics* 18, S58-S76
25. Almazi, J. G., Pockney, P., Gedye, C., Smith, N. D., Hondermarck, H., Verrills, N. M., and Dun, M. D. (2018) Cell-Free DNA Blood Collection Tubes Are Appropriate for Clinical Proteomics: A Demonstration in Colorectal Cancer. *Proteomics Clin Appl* 12, e1700121
26. Wiredja, D. D., Koyutürk, M., and Chance, M. R. (2017) The KSEA App: a web-based tool for kinase activity inference from quantitative phosphoproteomics. *Bioinformatics* 33, 3489-3491
27. Hornbeck, P. V., Zhang, B., Murray, B., Kornhauser, J. M., Latham, V., and Skrzypek, E. (2015) PhosphoSitePlus, 2014: mutations, PTMs and recalibrations. *Nucleic Acids Res* 43, D512-520
28. Wilhelm, S., Carter, C., Lynch, M., Lowinger, T., Dumas, J., Smith, R. A., Schwartz, B., Simantov, R., and Kelley, S. (2006) Discovery and development of sorafenib: a multikinase inhibitor for treating cancer. *Nat Rev Drug Discov* 5, 835-844
29. Golding, S. E., Rosenberg, E., Valerie, N., Hussaini, I., Frigerio, M., Cockcroft, X. F., Chong, W. Y., Hummersone, M., Rigoreau, L., Menear, K. A., O'Connor, M. J., Povirk, L. F., van Meter, T., and Valerie, K. (2009) Improved ATM kinase inhibitor KU-60019 radiosensitizes glioma cells, compromises insulin, AKT and ERK prosurvival signaling, and inhibits migration and invasion. *Mol Cancer Ther* 8, 2894-2902
30. BLISS, C. I. (1939) THE TOXICITY OF POISONS APPLIED JOINTLY1. *Annals of Applied Biology* 26, 585-615
31. Heberle, H., Meirelles, G. V., da Silva, F. R., Telles, G. P., and Minghim, R. (2015) InteractiVenn: a web-based tool for the analysis of sets through Venn diagrams. *BMC Bioinformatics* 16, 169
32. Olsen, J. V., Blagoev, B., Gnad, F., Macek, B., Kumar, C., Mortensen, P., and Mann, M. (2006) Global, In Vivo, and Site-Specific Phosphorylation Dynamics in Signaling Networks. *Cell* 127, 635-648
33. Mathew, N. R., Baumgartner, F., Braun, L., O'Sullivan, D., Thomas, S., Waterhouse, M., Müller, T. A., Hanke, K., Taromi, S., Apostolova, P., Illert, A. L., Melchinger, W., Duquesne, S., Schmitt-Graeff, A., Osswald, L., Yan, K.-L., Weber, A., Tugues, S., Spath, S., Pfeifer, D., Follo, M., Claus, R., Lübbert, M., Rummelt, C., Bertz, H., Wäsch, R., Haag, J., Schmidts, A., Schultheiss, M., Bettinger, D., Thimme, R., Ullrich, E., Tanriver, Y., Vuong, G. L., Arnold, R., Hemmati, P., Wolf, D., Ditschkowski, M., Jilg, C., Wilhelm, K., Leiber, C., Gerull, S., Halter, J., Lengerke, C., Pabst, T., Schroeder, T., Kobbe, G., Rösler, W., Doostkam, S., Meckel, S., Stabla, K., Metzelder, S. K., Halbach, S., Brummer, T., Hu, Z., Dengjel, J., Hackanson, B., Schmid, C., Holtick, U., Scheid, C., Spyridonidis, A., Stölzel, F., Ordemann, R., Müller, L. P., Sicre-de-Fontbrune, F., Ihorst, G., Kuball, J., Ehlert, J. E., Feger, D., Wagner, E.-M., Cahn, J.-Y., Schnell, J., Kuchenbauer, F., Bunjes, D., Chakraverty, R., Richardson, S., Gill, S., Kröger, N., Ayuk, F., Vago, L., Ciceri, F., Müller, A. M., Kondo, T., Teshima, T., Klaeger, S., Kuster, B., Kim, D., Weisdorf, D., van der Velden, W., Dörfel, D., Bethge, W., Hilgendorf, I., Hochhaus, A., Andrieux, G., Börries, M., Busch, H., Magenau, J., Reddy, P., Labopin, M., Antin, J. H., Henden, A. S., Hill, G. R., Kennedy, G. A., Bar, M., Sarma, A., McLornan, D., Mufti, G., Oran, B., Rezvani, K., Shah, O., Negrin, R. S., Nagler, A., Prinz, M., Burchert, A., Neubauer, A., Beelen, D., Mackensen, A., von Bubnoff,

693 N., Herr, W., Becher, B., Socié, G., Caligiuri, M. A., Ruggiero, E., Bonini, C., Häcker, G., Duyster, J., Finke, J., Pearce,
694 E., Blazar, B. R., and Zeiser, R. (2018) Sorafenib promotes graft-versus-leukemia activity in mice and humans
695 through IL-15 production in FLT3-ITD-mutant leukemia cells. *Nature Medicine* 24, 282-291
696 34. Antar, A., Kharfan-Dabaja, M. A., Mahfouz, R., and Bazarbachi, A. (2015) Sorafenib Maintenance Appears
697 Safe and Improves Clinical Outcomes in FLT3-ITD Acute Myeloid Leukemia After Allogeneic Hematopoietic Cell
698 Transplantation. *Clinical Lymphoma Myeloma and Leukemia* 15, 298-302
699 35. Chen, Y.-B., Li, S., Lane, A. A., Connolly, C., Del Rio, C., Valles, B., Curtis, M., Ballen, K., Cutler, C., Dey, B. R.,
700 El-Jawahri, A., Fathi, A. T., Ho, V. T., Joyce, A., McAfee, S., Rudek, M., Rajkhowa, T., Verselis, S., Antin, J. H., Spitzer,
701 T. R., Levis, M., and Soiffer, R. (2014) Phase I Trial of Maintenance Sorafenib after Allogeneic Hematopoietic Stem
702 Cell Transplantation for Fms-like Tyrosine Kinase 3 Internal Tandem Duplication Acute Myeloid Leukemia. *Biology*
703 *of Blood and Marrow Transplantation* 20, 2042-2048
704 36. Brunner, A. M., Li, S., Fathi, A. T., Wadleigh, M., Ho, V. T., Collier, K., Connolly, C., Ballen, K. K., Cutler, C. S.,
705 Dey, B. R., El-Jawahri, A., Nikiforow, S., McAfee, S. L., Koreth, J., Deangelo, D. J., Alyea, E. P., Antin, J. H., Spitzer, T.
706 R., Stone, R. M., Soiffer, R. J., and Chen, Y.-B. (2016) Haematopoietic cell transplantation with and without
707 sorafenib maintenance for patients with FLT3-ITD acute myeloid leukaemia in first complete remission. *British*
708 *Journal of Haematology* 175, 496-504
709 37. Tarlock, K., Chang, B., Cooper, T., Gross, T., Gupta, S., Neudorf, S., Adlard, K., Ho, P. A., McGoldrick, S.,
710 Watt, T., Templeman, T., Sisler, I., Garee, A., Thomson, B., Woolfrey, A., Estey, E., Meshinchi, S., and Pollard, J. A.
711 (2015) Sorafenib treatment following hematopoietic stem cell transplant in pediatric FLT3/ITD acute myeloid
712 leukemia. *Pediatric Blood & Cancer* 62, 1048-1054
713 38. Burchert, A., Bug, G., Fritz, L. V., Finke, J., Stelljes, M., Röllig, C., Wollmer, E., Wäsch, R., Bornhäuser, M.,
714 Berg, T., Lang, F., Ehninger, G., Serve, H., Zeiser, R., Wagner, E.-M., Kröger, N., Wolschke, C., Schleuning, M., Götze,
715 K. S., Schmid, C., Crysandt, M., Eßeling, E., Wolf, D., Wang, Y., Böhm, A., Thiede, C., Haferlach, T., Michel, C.,
716 Bethge, W., Wündisch, T., Brandts, C., Harnisch, S., Wittenberg, M., Hoeffkes, H.-G., Rospleszcz, S., Burchardt, A.,
717 Neubauer, A., Brugger, M., Strauch, K., Schade-Brittinger, C., and Metzelder, S. K. (2020) Sorafenib Maintenance
718 After Allogeneic Hematopoietic Stem Cell Transplantation for Acute Myeloid Leukemia With FLT3–Internal Tandem
719 Duplication Mutation (SORMAIN). *Journal of Clinical Oncology* 38, 2993-3002
720 39. Xuan, L., Wang, Y., Huang, F., Fan, Z., Xu, Y., Sun, J., Xu, N., Deng, L., Li, X., Liang, X., Luo, X., Shi, P., Liu, H.,
721 Wang, Z., Jiang, L., Yu, C., Zhou, X., Lin, R., Chen, Y., Tu, S., Huang, X., and Liu, Q. (2020) Sorafenib maintenance in
722 patients with FLT3-ITD acute myeloid leukaemia undergoing allogeneic haematopoietic stem-cell
723 transplantation: an open-label, multicentre, randomised phase 3 trial. *The Lancet Oncology* 21, 1201-1212
724 40. Maurer, G., Tarkowski, B., and Baccarini, M. (2011) Raf kinases in cancer–roles and therapeutic
725 opportunities. *Oncogene* 30, 3477-3488
726 41. Braicu, C., Buse, M., Busuioc, C., Drula, R., Gulei, D., Raduly, L., Rusu, A., Irimie, A., Atanasov, A. G., Slaby,
727 O., Ionescu, C., and Berindan-Neagoe, I. (2019) A Comprehensive Review on MAPK: A Promising Therapeutic Target
728 in Cancer. *Cancers (Basel)* 11
729 42. Zhu, Y. J., Zheng, B., Wang, H. Y., and Chen, L. (2017) New knowledge of the mechanisms of sorafenib
730 resistance in liver cancer. *Acta Pharmacol Sin* 38, 614-622
731 43. Mantovani, F., Collavin, L., and Del Sal, G. (2019) Mutant p53 as a guardian of the cancer cell. *Cell Death &*
732 *Differentiation* 26, 199-212
733 44. Xia, L., Tan, S., Zhou, Y., Lin, J., Wang, H., Oyang, L., Tian, Y., Liu, L., Su, M., Wang, H., Cao, D., and Liao, Q.
734 (2018) Role of the NFκB-signaling pathway in cancer. *Onco Targets Ther* 11, 2063-2073
735 45. Lavin, M. F. (2008) Ataxia-telangiectasia: from a rare disorder to a paradigm for cell signalling and cancer.
736 *Nature Reviews Molecular Cell Biology* 9, 759-769
737 46. Derheimer, F. A., and Kastan, M. B. (2010) Multiple roles of ATM in monitoring and maintaining DNA
738 integrity. *FEBS Lett* 584, 3675-3681
739 47. Sillar, J. R., Germon, Z. P., Deluliis, G. N., and Dun, M. D. (2019) The Role of Reactive Oxygen Species in
740 Acute Myeloid Leukaemia. *Int J Mol Sci* 20
741 48. Stanicka, J., Russell, E. G., Woolley, J. F., and Cotter, T. G. (2015) NADPH oxidase-generated hydrogen
742 peroxide induces DNA damage in mutant FLT3-expressing leukemia cells. *J Biol Chem* 290, 9348-9361
743 49. Sallmyr, A., Fan, J., Datta, K., Kim, K.-T., Grosu, D., Shapiro, P., Small, D., and Rassool, F. (2008) Internal
744 tandem duplication of FLT3 (FLT3/ITD) induces increased ROS production, DNA damage, and misrepair:
745 implications for poor prognosis in AML. *Blood* 111, 3173-3182

50. Mannan, A., Germon, Z. P., Chamberlain, J., Sillar, J. R., Nixon, B., and Dun, M. D. (2021) Reactive Oxygen Species in Acute Lymphoblastic Leukaemia: Reducing Radicals to Refine Responses. *Antioxidants (Basel)* 10

51. Corsello, S. M., Nagari, R. T., Spangler, R. D., Rossen, J., Kocak, M., Bryan, J. G., Humeidi, R., Peck, D., Wu, X., Tang, A. A., Wang, V. M., Bender, S. A., Lemire, E., Narayan, R., Montgomery, P., Ben-David, U., Garvie, C. W., Chen, Y., Rees, M. G., Lyons, N. J., McFarland, J. M., Wong, B. T., Wang, L., Dumont, N., O'Hearn, P. J., Stefan, E., Doench, J. G., Harrington, C. N., Greulich, H., Meyerson, M., Vazquez, F., Subramanian, A., Roth, J. A., Bittker, J. A., Boehm, J. S., Mader, C. C., Tsherniak, A., and Golub, T. R. (2020) Discovering the anticancer potential of non-oncology drugs by systematic viability profiling. *Nature Cancer* 1, 235-248

52. Ting, L., Rad, R., Gygi, S. P., and Haas, W. (2011) MS3 eliminates ratio distortion in isobaric multiplexed quantitative proteomics. *Nature Methods* 8, 937-940

53. Karp, N. A., Huber, W., Sadowski, P. G., Charles, P. D., Hester, S. V., and Lilley, K. S. (2010) Addressing accuracy and precision issues in iTRAQ quantitation. *Mol Cell Proteomics* 9, 1885-1897

54. Thingholm, T. E., Palmisano, G., Kjeldsen, F., and Larsen, M. R. (2010) Undesirable Charge-Enhancement of Isobaric Tagged Phosphopeptides Leads to Reduced Identification Efficiency. *Journal of Proteome Research* 9, 4045-4052

55. Pichler, P., Köcher, T., Holzmann, J., Mazanek, M., Taus, T., Ammerer, G., and Mechtler, K. (2010) Peptide Labeling with Isobaric Tags Yields Higher Identification Rates Using iTRAQ 4-Plex Compared to TMT 6-Plex and iTRAQ 8-Plex on LTQ Orbitrap. *Analytical Chemistry* 82, 6549-6558

56. Choudhary, C., Schwäble, J., Brandts, C., Tickenbrock, L., Sargin, B., Kindler, T., Fischer, T., Berdel, W. E., Müller-Tidow, C., and Serve, H. (2005) AML-associated Flt3 kinase domain mutations show signal transduction differences compared with Flt3 ITD mutations. *Blood* 106, 265-273

57. Lavin, M. F., and Yeo, A. J. (2020) Clinical potential of ATM inhibitors. *Mutat Res* 821, 111695

58. Golding, S. E., Rosenberg, E., Adams, B. R., Wignarajah, S., Beckta, J. M., O'Connor, M. J., and Valerie, K. (2012) Dynamic inhibition of ATM kinase provides a strategy for glioblastoma multiforme radiosensitization and growth control. *Cell Cycle* 11, 1167-1173

59. Frosina, G., Ravetti, J. L., Corvò, R., Fella, M., Garrè, M. L., Levrero, F., Marcello, D., Marubbi, D., Morana, G., Mussap, M., Neumaier, C. E., Profumo, A., Raso, A., Rosa, F., Vagge, S., Vecchio, D., Verrico, A., Zona, G., and Daga, A. (2018) Faithful animal modelling of human glioma by using primary initiating cells and its implications for radiosensitization therapy. *Scientific Reports* 8, 14191

60. Golding, S. E., Rosenberg, E., Neill, S., Dent, P., Povirk, L. F., and Valerie, K. (2007) Extracellular signal-related kinase positively regulates ataxia telangiectasia mutated, homologous recombination repair, and the DNA damage response. *Cancer Res* 67, 1046-1053

61. Coriat, R., Nicco, C., Chéreau, C., Mir, O., Alexandre, J., Ropert, S., Weill, B., Chaussade, S., Goldwasser, F., and Batteux, F. (2012) Sorafenib-induced hepatocellular carcinoma cell death depends on reactive oxygen species production in vitro and in vivo. *Mol Cancer Ther* 11, 2284-2293

62. Wong, M., Mayoh, C., Lau, L. M. S., Khuong-Quang, D. A., Pinese, M., Kumar, A., Barahona, P., Wilkie, E. E., Sullivan, P., Bowen-James, R., Syed, M., Martincorena, I., Abascal, F., Sherstyuk, A., Bolanos, N. A., Baber, J., Priestley, P., Dolman, M. E. M., Fleuren, E. D. G., Gauthier, M. E., Mould, E. V. A., Gayevskiy, V., Gifford, A. J., Grebert-Wade, D., Strong, P. A., Manouvrier, E., Warby, M., Thomas, D. M., Kirk, J., Tucker, K., O'Brien, T., Alvaro, F., McCowage, G. B., Dalla-Pozza, L., Gottardo, N. G., Tapp, H., Wood, P., Khaw, S. L., Hansford, J. R., Moore, A. S., Norris, M. D., Trahair, T. N., Lock, R. B., Tyrrell, V., Haber, M., Marshall, G. M., Ziegler, D. S., Ekert, P. G., and Cowley, M. J. (2020) Whole genome, transcriptome and methylome profiling enhances actionable target discovery in high-risk pediatric cancer. *Nat Med* 26, 1742-1753

63. Perez-Riverol, Y., Csordas, A., Bai, J., Bernal-Llinares, M., Hewapathirana, S., Kundu, D. J., Inuganti, A., Griss, J., Mayer, G., Eisenacher, M., Pérez, E., Uszkoreit, J., Pfeuffer, J., Sachsenberg, T., Yilmaz, S., Tiwary, S., Cox, J., Audain, E., Walzer, M., Jarnuczak, A. F., Ternent, T., Brazma, A., and Vizcaíno, J. A. (2019) The PRIDE database and related tools and resources in 2019: improving support for quantification data. *Nucleic Acids Res* 47, D442-d450

FIGURE CAPTIONS

Figure 1: Overview of sample preparation and instrument workflow to compare quantitative phosphoproteomics using TMT and pHASED. Proteins were extracted from target cell lines and digested into peptides. *A)* One hundred micrograms of peptide/sample was labeled with TMT 10-plex isobaric tags, mixed 1:1, and enriched for phosphopeptides prior to offline HILIC fractionation and analysis on a Q Exactive Orbitrap MS. *B)* In the optimized pHASED workflow, two hundred micrograms of digested peptides were separated for enrichment. Known concentrations of spike-in heavy labeled phosphopeptides were added to each sample prior to phosphopeptide enrichment, and enriched phosphopeptides were then injected into an Orbitrap Exploris 480 coupled with a FAIMS interface using four different compensation voltages (CVs; -70V, -60V, -50V and -40V). Figure created with BioRender.com.

Figure 2. Acquisition profile of phosphopeptide-spectrum matches (PSMs) resulting from TMT compared to pHASED. *A)* Percentage of charge states of all peptide ions selected for MS/MS in TMT and pHASED experiments. *B)* Distribution of precursor ions identified in each experiment, stratified according to m/z. *C*) Percentage of PSMs identified in each CV. *D*) Average m/z of all PSM features acquired in each CV. *E*) Average m/z of PSM features for charge states acquired in each CV. *F*) Venn distribution of unique phosphoprotein accessions identified in CVs -70V, -60V, -50V and -40V shows overall coverage of common and unique acquisitions detected in each CV. Venn diagram created with InteractiVenn.

Figure 3. **Quantification reproducibility between biological replicates TMT and pHASED experiments.** Pearson correlation profiles for biological replicates (n=3) of six isogenic models of acute myeloid leukemia analyzed by *A*) TMT, and *B*) pHASED label-free experiments. *C*) Heatmap comparison of all three correlation scores achieved by from isogenic cell line for TMT

and pHASED. Correlation was performed using normalized abundances in Perseus, and graphs were plotted using GraphPad Prism 8.4.3.

Figure 4. Analysis of phosphoproteome coverage and phosphopeptide characteristics identified using TMT compared with pHASED. *A)* Summary of MS acquisition comparing TMT and pHASED experiments. *B)* Number of single and multi-phosphorylated peptides identified in each experiment comparing TMT and pHASED. *C*) Phosphoprotein coverage comparing TMT and pHASED experiments. *D*) Number of phosphopeptides per protein identified in TMT and pHASED experiments. *E*) Overlap of phosphoprotein accessions comparing TMT and pHASED experiments. *F)* GRAVY score of peptides identified in each TMT and pHASED experiment irrespective of PTMs. *G)* Median distribution of log2 ratios for phosphopeptide changes in FLT3 mutants (S2-S6) compared to FLT3-wt (S1) in TMT and pHASED experiments. *H*) Number of phosphorylated master protein kinases identified in each TMT and pHASED experiment ($p<0.01$).

Figure 5. **Comparison of phosphorylated kinases identified in resistant cell lines comparing TMT and pHASED experiments.** *A*) Cell viability was assessed by resazurin assay at 48 h following treatment with sorafenib in FLT3-ITD, FLT3-ITD/D835V, and FLT3-ITD/D835Y isogenic cell lines (n=3 independent replicates). *B*) Number of kinases identified as differentially phosphorylated ($\log_2 \pm 0.25$) in double mutants in comparison to FLT3-ITD cell using TMT and pHASED datasets. *C*) Kinases with significantly increased or decreased phosphorylation ($\log_2 \pm 0.25$; $p<0.05$) in resistant cell lines comparison to FLT3-ITD identified by TMT and pHASED. Functional protein-protein interaction network and enrichment profile of kinases differentially phosphorylated ($\log_2 \pm 0.25$) in resistant cell lines compared to FLT3-ITD cells. Protein interaction network shown corresponding to the major cluster of kinases identified in *D*) FLT3-

ITD/D835V via pHASED; *E*) FLT3-ITD/D835V via TMT; and *F*) FLT3-ITD/D835Y via pHASED, and *G*) FLT3-ITD/D835Y via TMT. Yellow indicates increased phosphorylation, whereas Blue represents decreased phosphorylation. Canonical pathways of enriched kinases (Purple = FLT3-ITD/D835V, Blue = FLT3-ITD/D835Y) with FDR <1% in each comparison are also shown.

Figure 6. **Bioinformatic analysis of FLT3 resistant phenotype via pHASED.** *A*) Kinase substrate enrichment analysis (KSEA) profile of resistant cell lines compared to FLT3-ITD. Z score indicates predicted kinase activity, with a positive value predictive of kinase activation and a negative value predictive of kinase inhibition. *B)* Ingenuity Pathway analysis (IPA) of phosphorylated changes in resistant cell lines compared with FLT3-ITD. *C*) Phosphorylation profile of ATM substrates in resistant cell lines compared with FLT3-ITD. Yellow indicates increased phosphorylation, whereas Blue represents decreased phosphorylation. Missing values are colored Grey. Phosphorylation profile of substrates downstream DSB repair pathway for *D*) FLT3-ITD/D835V and *E*) FLT3-ITD/D835Y compared with FLT3-ITD. Statistical significance calculated via one-way ANOVA with significant threshold of **p*<0.05, ***p*<0.01 and ****p*<0.001.

Figure 7. **Sensitivity to ATM inhibition (KU-60019) in combination with FLT3 inhibitor sorafenib.** Bliss synergy analysis of combined effect of sorafenib and KU-60019 in *A)* FLT3-ITD/D835Y, *B)* FLT3-ITD/D835V, and *C)* FLT3-ITD (<0= antagonistic, >0<10=additive, >10=synergistic). Cell survival comparison of *D*) FLT3-ITD/D835Y, and *E*) FLT3-ITD/D835V cell lines at 62 nM sorafenib in combination with 1.25 µM, 2.5 µM and 5 µM KU-60019 (n=3 independent replicates). Statistical significance calculated via one-way ANOVA with significant threshold of **p*<0.05, ***p*<0.01 and ****p*<0.001.

865

866 **TABLES**

867 **Table 1:** Isogenic cellular models of FLT3 mutant AML analyzed by TMT and pHASED

868 protocols in biological triplicate ((n=36/technique)

Cell line	Species	Biological replicates	Samples	Model of AML stage	Sorafenib sensitivity
FDC-P1	Mouse	3	FLT3wt	Normal	Sensitive
FDC-P1	Mouse	3	FLT3-ITD	Diagnosis	Sensitive
FDC-P1	Mouse	3	FLT3-D835V	Diagnosis	Sensitive
FDC-P1	Mouse	3	FLT3-D835Y	Diagnosis	Sensitive
FDC-P1	Mouse	3	FLT3-ITD/D835V	Relapse	Resistant
FDC-P1	Mouse	3	FLT3-ITD/D835Y	Relapse	Resistant

869

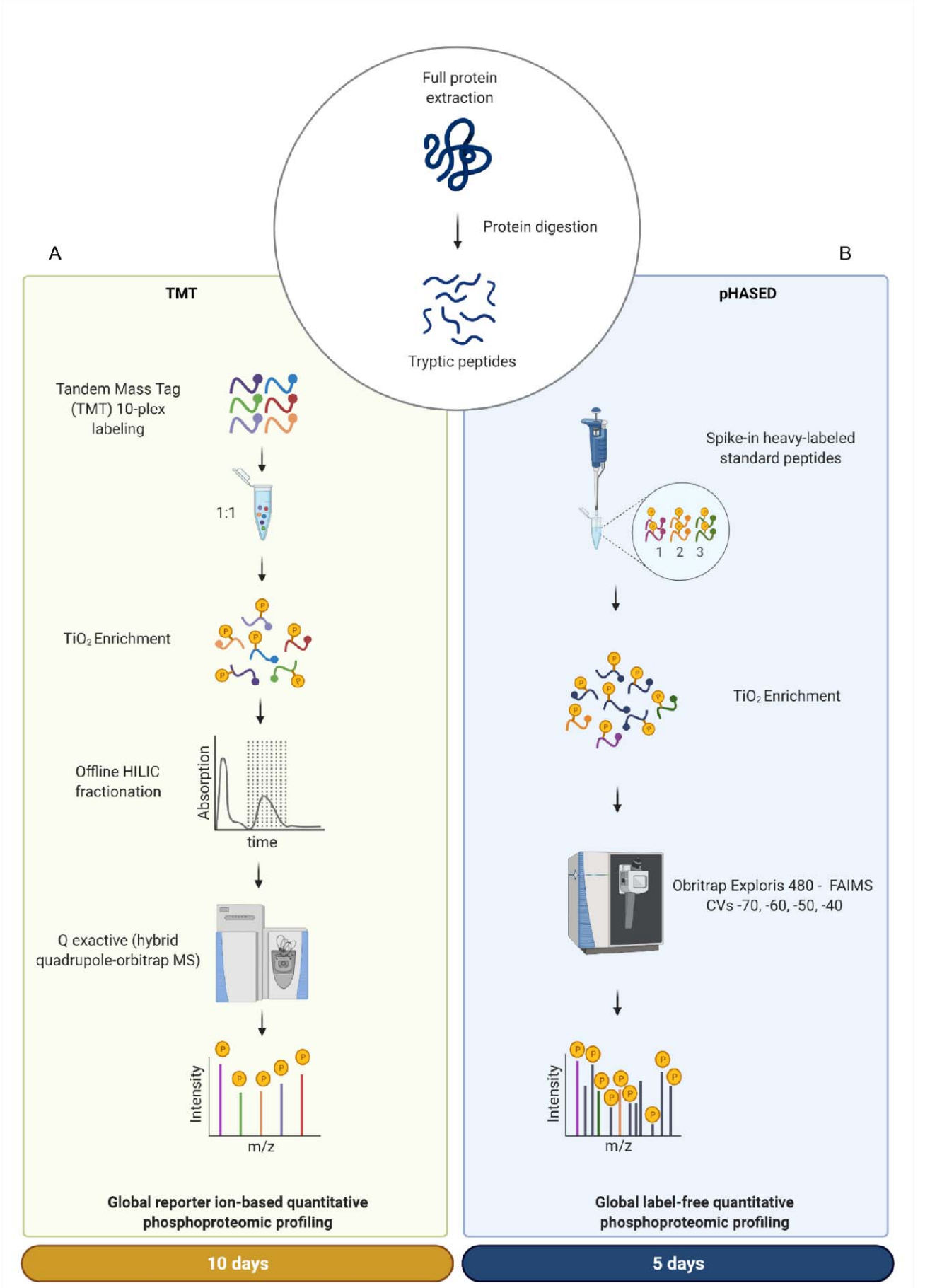

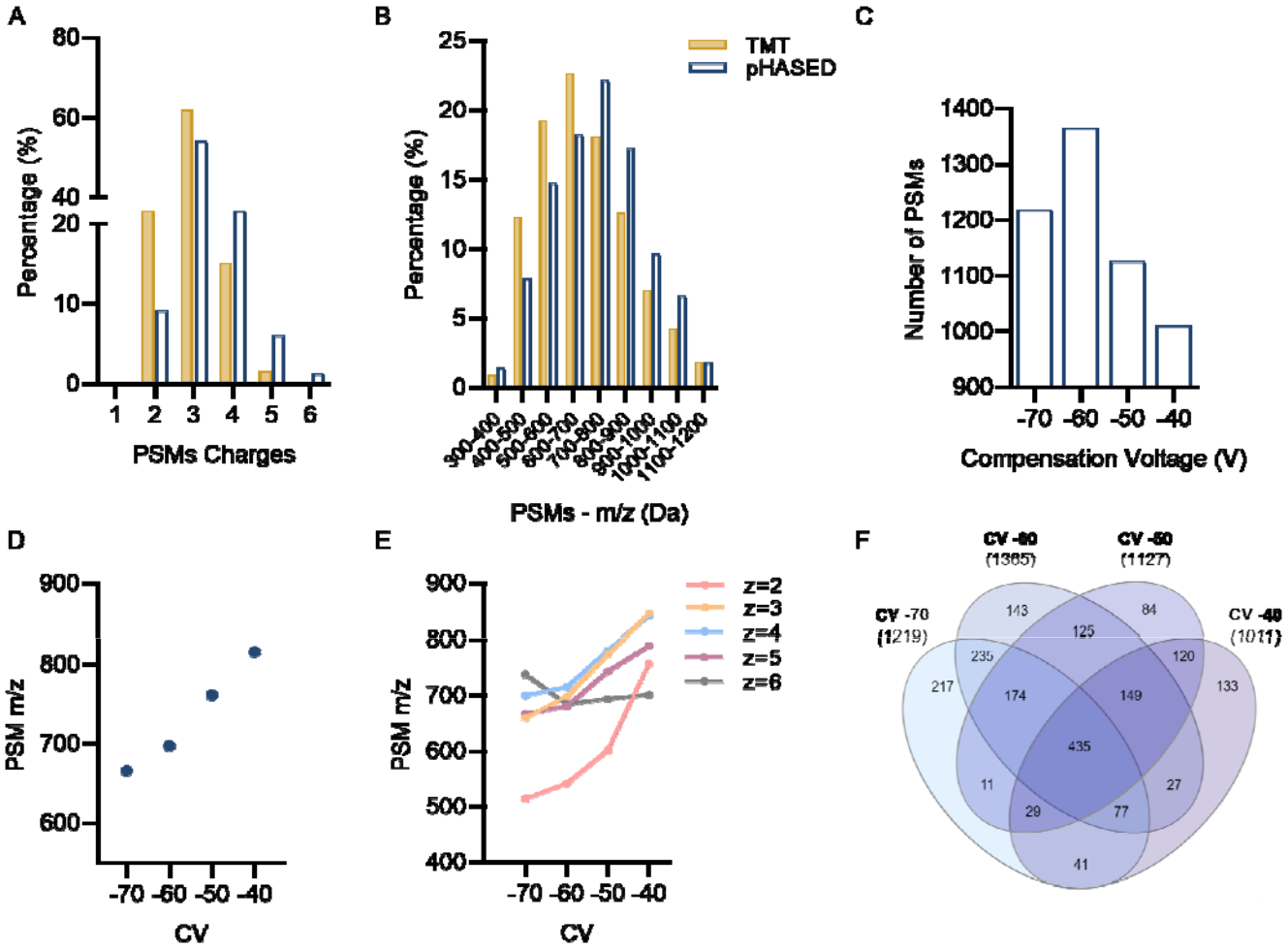

A

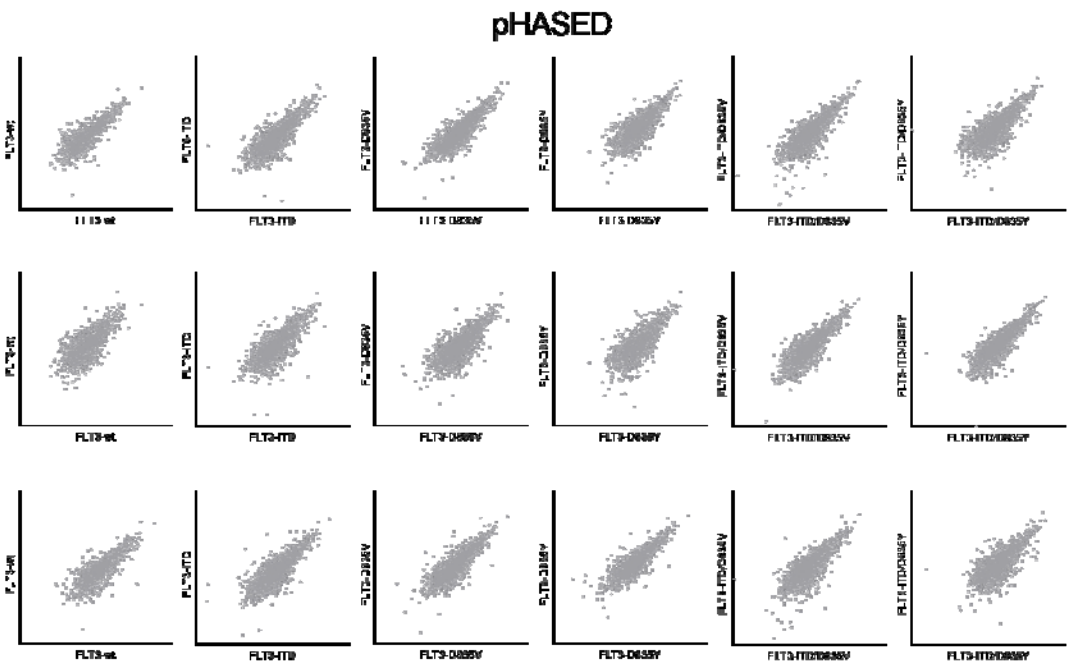

B

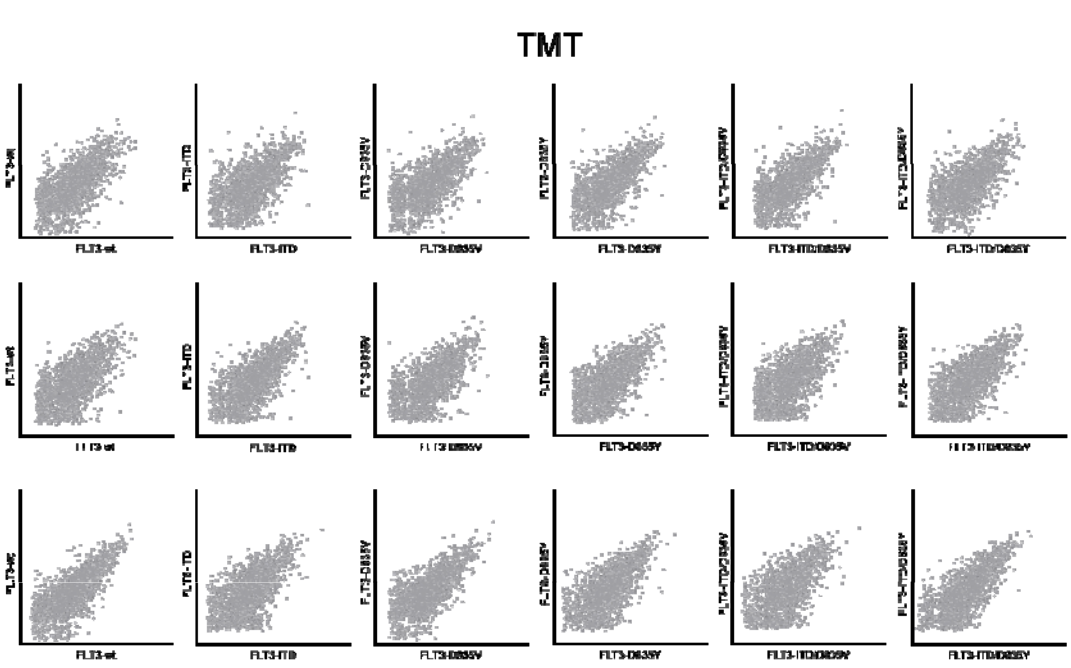

C

Sample	FLT3-wt			FLT3-ITD			FLT3-D835V			FLT3-D835Y			FLT3-ITD/D835V			FLT3-ITD/D835Y		
pHASED	0.71	0.81	0.83	0.85	0.76	0.75	0.78	0.85	0.85	0.75	0.86	0.78	0.85	0.79	0.83	0.85	0.76	0.75
TMT	0.64	0.62	0.75	0.62	0.69	0.66	0.64	0.64	0.72	0.68	0.67	0.67	0.67	0.60	0.60	0.65	0.66	0.72

weak moderate strong

A

Method	TMT	pHASED
PSMs	32,241	133,855
# pPRO	1,958	1,587
# pPEP	3,861	7,694
S:T:Y ratio (%)	89:10:1	82:16:2
Enrichment (%)	72	93